Growth of a TiO_2 nanotubular layer without presence of nanograss in a short time

M. Luna Cervantes, A. Báez Rodríguez, J. Hernández Torres, and L. Zamora Peredo
Centro de Investigación en Micro y Nanotecnología, Universidad Veracruzana, Adolfo Ruiz Cortines 455, 94294, Boca del Río, México.

Received 3 August 2018 ; accepted 14 September 2018

Many studies, focused in TiO_2 anodized, uses frequently a NH_4F salt concentration from 0.3- 0.5 wt% and the whole information about how voltage, time and even pH affects to nanotubes morphology, are effective just for these concentration range. It is known that increasing salt concentration, the electrolyte increases their conductivity and anodization speed (oxidation-dissolution) suffers also an increment and for a specifically concentration 1.2wt%, there is no data about morphology repercussions. A TiO_2 nanotubular matrix is synthesized, in order to identify the range of time where it is possible to obtain with no presence of nanograss. The anodization process consists of an organic electrolyte of ethylene glycol, deionized water and 1.2 wt% NH_4F salts, constant potential of 30 V, and a time lapse from 10 to 60 minutes (short time). All anodized samples are rinsed and annealed to 400°C for 4 hours to obtain an anatase crystalline structure; no samples are cleaned in ultrasonic bath to preserve the nanograss structure. Optical characterization was performed by Raman Spectroscopy to identify the increases in signal intensity, associated with thickness. The morphological characterization was carried out by Scanning Electron Microscopy to verify the presence and density of the nanograss and nanotubes.

Keywords: TiO_2; nanotube; nanograss; anatase; anodization; Raman; SEM.

PACS: 61.46.Fg; 62.23.-c; 81.07.De; 82.45.Cc; 82.45.Yz.

1. Introduction

Titanium dioxide material has been studied and used in areas like dye sensitized solar cells [1], hydrogen generation by water photo electrolysis [2], photocatalytic reduction of CO_2 under outdoor sunlight [3], super capacitors [4], batteries [5], biomedical related applications including biosensors, molecular filtration, drug delivery, and tissue engineering [6-8], because of the particular properties of TiO_2 such as nontoxic, environmentally friendly, optical and electronic properties [9].

The high volume-area ratio, as a very important property of nanoscale [10], attracted significant attention from researchers, as it developed a new family of nanostructures, named for what they look like, *e.g.* nanorods, nanopores, nanowires, nanobelts and so on [11]. These structures can be obtained by physical and chemical synthesis methods [12-14]. There is one special type of nanostructure, which has in fact a double area by default (inner and outer), that offers one direct and efficient pathway for electron transport [15] and a double surface, available for nanoparticles insertion [16], they are called nanotubes [17].

TiO_2 nanotubes can be synthesized using anodic oxidation process (also called anodization), first reported in 2001 [14]. Anodization is an electrolytic process that creates a protective or decorative oxide layer. This versatile technique uses titanium (working as anode), usually foils, to obtain a vertically oriented nanotube matrix; the cathode is commonly a plate, rod or foil of pure platinum [18,19] even when this material is too expensive. The process starts when a potential is applied [20], the anodization usually takes hours [21]. The anodized samples are cleaned in an ultrasonic bath frequently [22], or another mechanical method is to remove the residual structures such as nanograss, sponge or just a very thin oxide layer [23], because prolonged time or high concentration of salts can cause them to appear [24], for general purposes they need to be removed, even when the nanotubes suffer some alteration in their shape or top layer surface. As-anodized oxide layer formed, it is amorphous in nature [25], generally, crystallization is achieved through thermal treatment at 350-500°C [26] in a variety of atmospheres for high performance applications with anatase phase [27-29]. For specific applications, electrolyte selection is very important [30], commonly used NH_4F salts and ethylene glycol due the biocompatibility in the biomedical field [30].

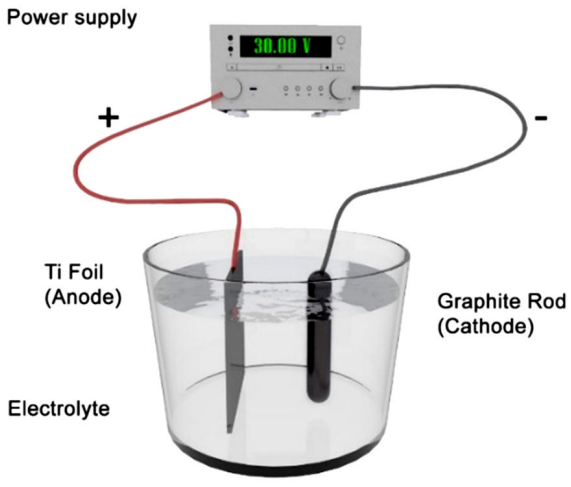

FIGURE 1. 3D Schematic diagram of the anodization set-up (two electrode configuration). Organic electrolyte consists of ethylene glycol, 2% deionized water and 1.2 wt% NH_4F.

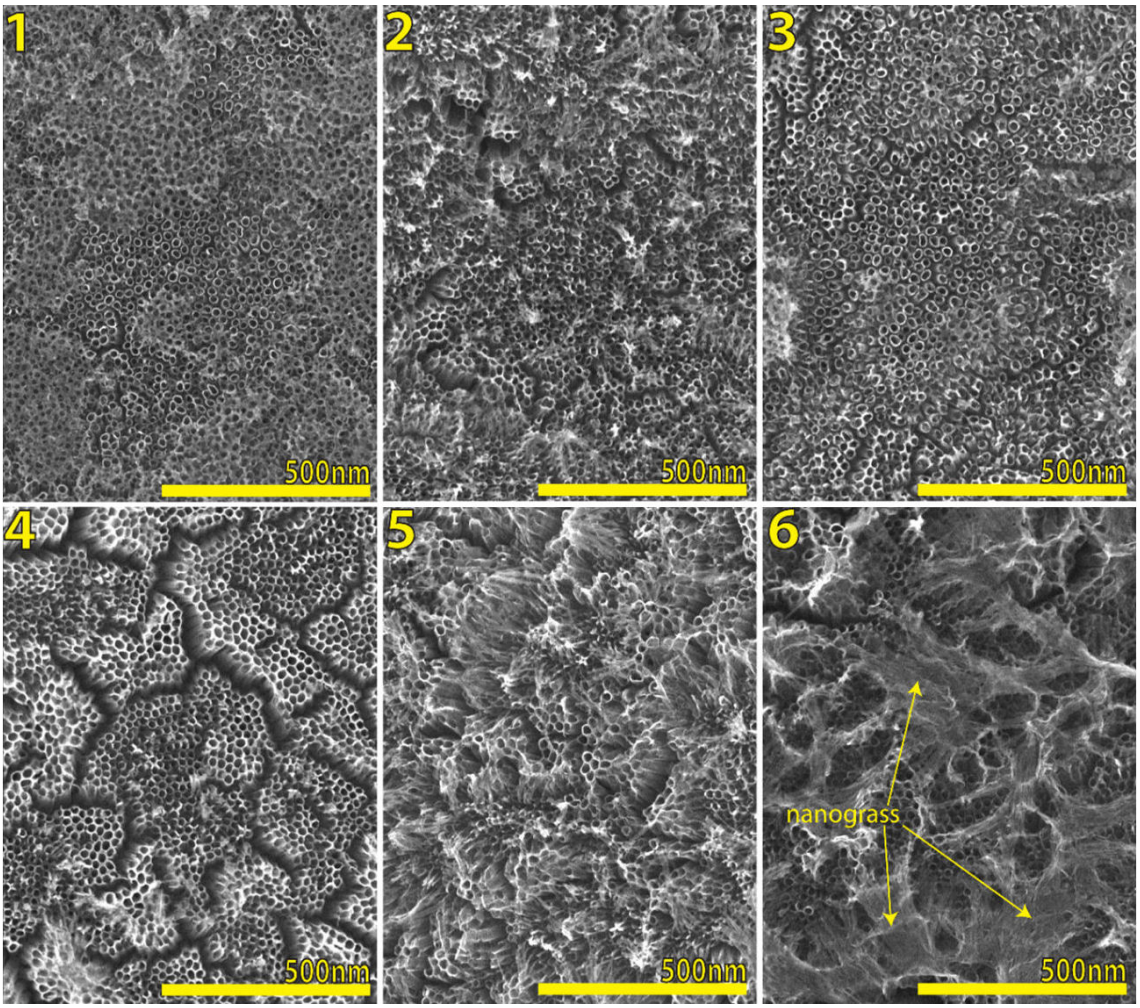

FIGURE 2. Scanning electron microscopy (SEM) micrographs of TiO_2 nanotube layers by anodization under constant voltage (30 V) in ethylene glycol, D.I. water and NH_4F, after annealing process. Anodization time of: 1) 10 min, 2) 20 min, 3) 30 min, 4) 40 min, 5) 50 min, 6) 60 min, here is indicated the nanograss presence.

The main goal in this study was to identify the time lapse in minutes, where a TiO_2 nanotubular matrix can be obtained with no presence of nanograss and exclude the ultrasonic bath or another mechanical method, in order to remove it. A good tube shape, a vertical alignment and a free top layer, are necessary characteristics for a better performance in almost all applications; moreover, an important factor in this study was the selection and use of graphite as an effective alternative cathode, due to low cost and optimal nanotube morphology.

2. Experimental

Titanium foils ($15 \times 15 \times 0.1$ mm) were firstly used as an anodic electrode, while pure graphite rods (35×6 mm) were used as cathodic electrode. Titanium foils were cut in smaller foils ($15 \times 5 \times 0.1$ mm), then they were cleaned by ultrasonication successively in ethanol, deionized water and acetone. The distance between electrodes was constant in every experiment (30 mm). The foils were anodized from 10 to 60 minutes in organic electrolyte: ethylene glycol, 2% deionized water and 1.2 wt% NH_4F; using two electrode configurations.

The anodization was carried out using a DC power source under constant voltage of 30 V, the schematic diagram of the anodization set-up is shown in Fig. 1.

After anodization process, the whole set of anodized samples was rinsed in deionized water, dried and then annealed at 400°C for 4 hours in air. The morphology and structure of TiO_2 nanostructure was characterized by Field Emission Scanning Electron Microscope (SEM) (JSM-7600F, JEOL), Raman spectra were obtained on a DXR Raman Microscope (Thermo Scientific) using a 532 nm laser, 50X objective, 10 mW power, 50 μm slit and 3 s time collection.

3. Results and discussion

At a first glance, Fig. 2 remarks how TiO2 nanotubes suffer a degeneration over a top layer surface. For more details, Fig. 2 shows in 1), 2) and 3) a good nanotube layer with a very little presence of residual thin oxide layer, it is formed in the first

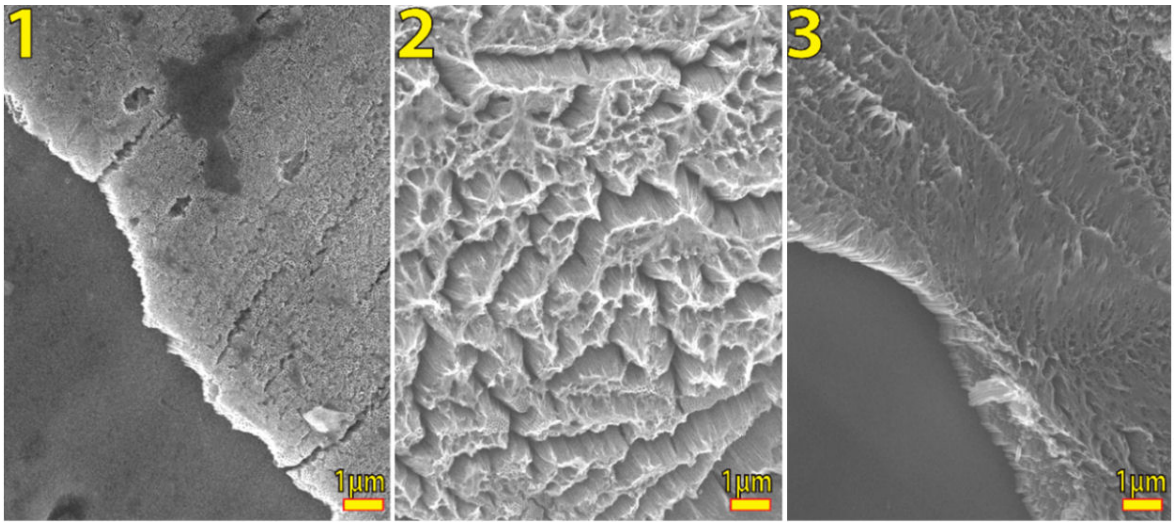

FIGURE 3. Perspective SEM micrographs of anodized samples by 1) 10 min, where there is just nanotube presence, 2) 30 min, where is clearly to see how the nanotubes are collapsed; 3) 60 min, there are a strong presence of nanograss.

stage of growth [31] for a time of 10, 20 and 30 minutes respectively, even this oxide layer can be easily removed when rinsed in D.I. water thoroughly, or Nitrogen beam, here the nanotube diameter is around 52-53 nanometers, which is a good size for insertion of nanoparticles for example, so it is very important to remark this time lapse where it is possible to have a good shape of tubes; 4) This micrograph demonstrates how the nanotubes start to collapse, forming clusters of bundled nanotubes (also called islands), this is due to the surface stress originating during formation of the oxide films [32] and an irregular topology of substrate; 5) here it is very clear to see how the nanotubes are collapsed due to be grown by extended anodizing time, often a disintegration of the top end of nanotubes due to chemical dissolution is observed, and then the nanotubes transform into TiO_2 nanograss [33,34]; 6) It clearly shows a full presence of well-formed nanograss, where the nanotube diameter is around 62-65 nanometers due to time progress under the same voltage, this diameter size is still suitable for general purpose.

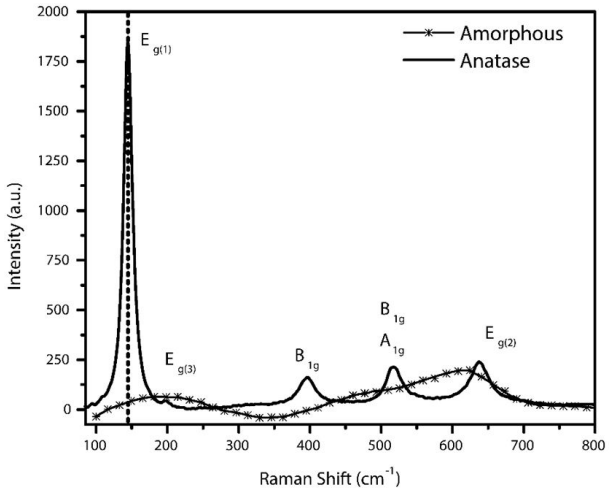

FIGURE 4. Raman Spectra of one anodized sample, dash line show as-anodized sample and after annealing treatment to 400°C with solid line. There are clearly visible as the six Raman active vibrational modes for anatase phase A_{1g}, $2B_{1g}$, $3E_g$.

The change from an amorphous state (as-anodized sample) to crystalline phase, as result after the annealing process to 400°C during 4 hours in air, can be confirm through Raman spectroscopy. As per literature report, there are six Raman active modes of anatase phase: A1g (515 cm^{-1}), 2B1g (400 and 519 cm^{-1}), 3Eg (144, 197 and 640 cm^{-1}) [35]. Figure 4 clearly shows the peaks obtained experimentally.

Figure 5 shows a close up from 130 to 156 cm^{-1} (1) with the whole set of Raman spectra (six anodized samples), it is possible to see and observe how the Raman intensity suffers an increment due to oxide thickness, it is progressive as a time function. There is a little change in Eg. (1) peak position, from a theoretical Raman shift 144 cm^{-1} (indicated by vertical red dashed line) for TiO_2 nanotubes films [36] and if this result is compared to SEM micrographs it is possible to observe how this vibrational mode appears with the bigger displacement of 1.1985 cm^{-1} for a anodization time of 10 minutes, and as we know based in Fig. 2, for this anodization time, there is just a vertically oriented nanotubes layer, very thin after all with a tube length of 335 nm; 20, 30, and 50 minutes exhibit a decrement about the shift; 40 and 60 minutes have an increment (blue shift) and we can associate it with the presence of nanotube islands and nanograss (Fig. 2). Alhomoudi *et al*. explained this relation between Eg shift, Raman intensity and oxide thickness, trough experimental and analytical study, it has been demonstrated that when thickness increases, the decreasing of Eg shift exists, until standard position (144 cm^{-1}) and this E_g Shift is due to stress between substrate and oxide layer [37] also it has been recognized that residual compressive stresses may cause film delamination from the substrate whereas tensile stress may

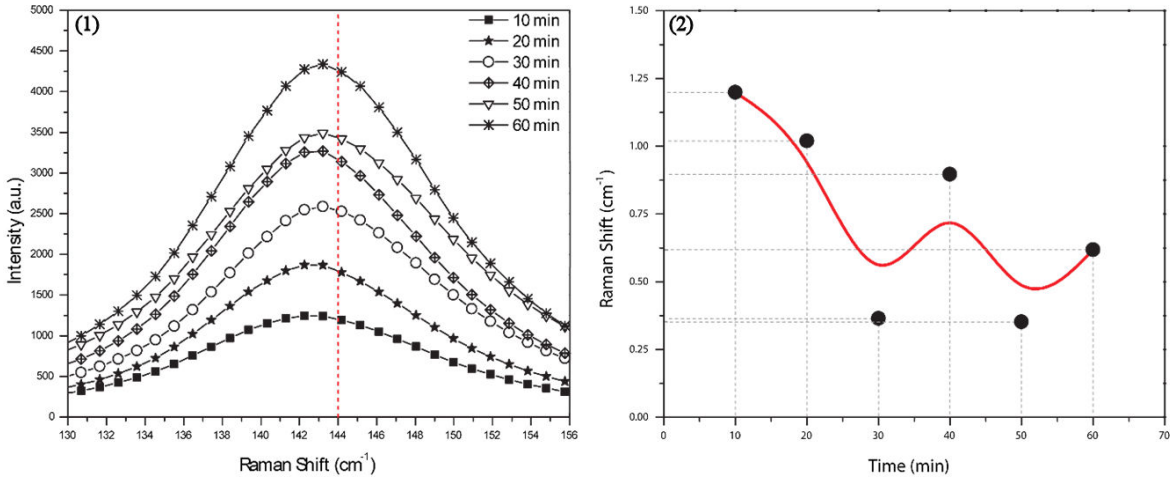

FIGURE 5. The whole set of anodized samples was analysed by Raman Spectroscopy. It is possible to identify a change in Eg(1) vibrational mode: Intensity due of the thickness (1) and Raman shift due to stress (2).

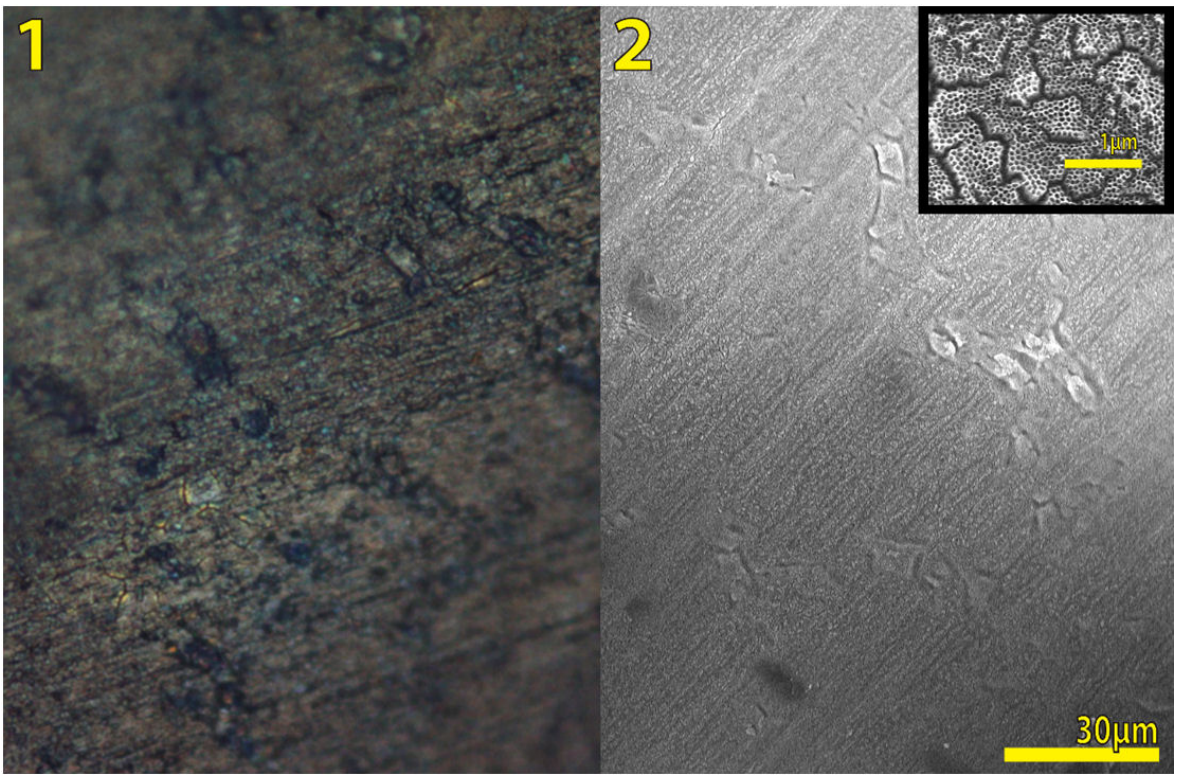

FIGURE 6. Raman micrography (1) to 20x and bright field, it is possible to observe some micro surface cracks; SEM micrography (2) to 800x and one inset where is possible appreciate very well the nanotube islands.

cause surface cracks in the film, similar to nanotube islands and micro surface cracks (Fig. 6). The dominant 144 cm^{-1} E_g mode is shifted towards a higher frequency by an amount that depends on the substrate as well as on the thickness of the film. The compressive stresses gradually increase with lower film thickness, which means that the stress gets higher closer to the film and substrate interface. The shifts of the 400 cm^{-1} B_{1g} and 640 cm^{-1} E_{1g} modes were toward lower wave numbers and decrease with film thickness. Similar behavior has been related to the confinement effects in nanostructured anatase crystallites [38-41].

4. Conclusion

Amorphous TiO_2 nanotube layers, produced by titanium anodic oxidation, can be studied and used for general purpose, but for high performance, and take advantage of more special features, this oxide layer can be crystallized into pure anatase

phase, through the annealing process under 350-500°C. As a main target to have nanotubes without presence of nanograss and with no use of cleaning mechanical procedures, a time lapse under specifically conditions (pH, electrolyte concentration, voltage and temperature) can be obtained from 10 to 30 minutes, even 40 minutes and still be a clean nanotube sample. Due to the time of anodizing and constant voltage, these nanotubes are sub-micrometric in size and these can be used to Surface Enhanced-Raman Spectroscopy applications without problem.

Acknowledgments

The authors are grateful to Centro de Investigación en Micro y Nanotecnología (MICRONA), Master of Science Daniel de Jesús Araujo Pérez, Engineer Rebeca Cristal Rodríguez Jiménez and Diana Balanyuk, for their help in this research.

1. M. Grätzel, *Nature* **414** (2001) 338-344.
2. W. Yang, *et al*., Nano Letters, **15** (2015) 7574-7580.
3. L. Tan, L. Ong, W. Chai, S. Mohamed, *Applied Catalysis B: Environmental* **166** (2015) 251-259.
4. Z. Gao, X. Zhu, Y. Li, X. Zhou, and Y. Song, *Chemical communications* **51** (2015) 7614-7617.
5. X. Liu, K. Wang, J. Chen, *Energy Storage Materials* **3** (2016) 1-17.
6. K. Popat, M. Eltgroth, T. LaTempa, C. Grimes, T. Desai, *Titania nanotubes: a novel platform for drug-eluting coatings for medical implants? Small* **11** (2007) 1878-1881.
7. K. Popat, L. Leoni, C. Grimes, T. Desai, *Biomaterials* **28** (2007) 3188-3197.
8. L. Peng, A. Mendelsohn, T. LaTempa, S. Yoriya, C. Grimes, T. Desai, *Nano Lett* **9** (2009) 1932-1936.
9. M. Fadlallah, *Physica E: Low-dimensional Systems and Nanostructures* **89** (2017) 50-56.
10. G. Guisbiers, *Nanoscale Research Letters* **5** (2010) 1132-1136.
11. M. Ge, *et al*., *Journal of Materials Chemistry A* **4** (2016) 6772-6801.
12. T. Kasuga, M. Hiramatsu, A. Hoson, T. Sekino, K. Niihara, *Advanced materials* **11** (1999) 1307-1311.
13. C. Nam, J. Falconer, L. Du, W. Yang, *Mater. Res. Bull.* **51** (2014) 49-55.
14. Gong, D; Grimes, C; Varghese, O; Hu, W; Singh, R; Chen, Z; Dickey, *E. J. Mater Res* **16** (2001) 3331.
15. B. Rao, A. Torabi, O. Varghese, *MRS Communications* **6** (2016) 375-396.
16. A. Lamberti, *et al*., *Journal of Materials Chemistry C* **3** (2015) 6868-6875.
17. Z. Sun, T. Liao, L. Kou, *Science China Materials* **60** (2016) 1-24.
18. R. Jin, M. Liao, T. Lin, S. Zhang, X. Shen, Y. Song, X. Zhu, *Materials Research Express* **4** (2017) 6.
19. M. Martínez, *et al*., *Molecules* (2017) 22 564.
20. K. Mor, O. Varghese, M. Paulose, K. Shankar, C. Grimes, *Solar Energy Materials and Solar Cells* **90** (2006) 2011-2075.
21. R. Chernozem, M. Surmeneva, R. Surmenev, *IOP Conf. Ser.: Mater. Sci. Eng* **116** (2016) 012025.
22. H. Prakasam, K. Shankar, M. Paulose, C. Grimes, *J Phys Chem C* **111** (2007) 7235-7241.
23. Q. Gui, D. Yu, D. Li, Y. Song, X. Zhu, L. Cao, S. Zhang, W. Ma, *Applied Surface Science* **314** (2014) 505-509.
24. T. Hoseinzadeh, Z. Ghorannevis, M. Ghoranneviss, *Appl. Phys. A* **123** (2017) 436.
25. J. Ya, A. Li,Z. Liu, E. Lei, W. Zhao, D. Zhao, C. Liu, *Journal of optoelectronics and advanced materials* **13** (2011) 684-688.
26. Y. Smith, R. Ray, K. Carlson, B. Sarma, M. Misra, *Materials* **6** (2013) 2892-2957.
27. X. Liu, J. Lin, Y. Tsang, X. Chen, P. Hing, H. Huang, *Journal of Alloys and Compounds* **607** (2014) 50-53.
28. J. Lin, X. Liu, S. Zhu, Y. Liu, X. Chen, *Nanoscale Res Lett* **10** (2015) 110.
29. N. Zec, N. Cvjeticanin, M. Bester, M. Vranes, S. Gadzuri, *Journal of The Electrochemical Society* **164** (2017) H5100-H5107.
30. K. Indira, U. Kamachi, T. Nishimura, N. Rajendran, *Journal of bio- and tribo-corrosion* **1** (2015) 28.
31. Y. Yin, Z. Jin, F. Hou, X. Wang, *J. Am. Ceram. Soc* **90** (2007) 2384-2389.
32. K. Zhu, T. Vinzant, N. Neale, *Nano Letters* **7** (2007) 3739-3746.
33. Y. Song, R. Lynch, D. Kim, P. Roy, P. Schmuki, *Electrochemical and Solid-State Letters* **12** (2009) C17-C20.
34. M. Paulose, *et al*., *J. Phys. Chem. B* **110** (2006) 16179-16184.
35. T. Ohsaka, F. Izumi, Y. Fuji, *Journal of Raman Spectroscopy* **7** (1978) 321-324.
36. G. Zakharova, *Russian Journal of Inorganic Chemistry* **59** (2014) 148-153.
37. I. Alhomoudi, G. Newaz, *Thin Solid Films* **517** (2009) 4372-4378.
38. S. Kelly, F. Pollak, M. Tomkiewicz, *The Journal of Physical Chemistry B* **101** (1997) 2730-2734.
39. Y. Mao, J. Wong, *Am. Chem. Soc.* **128** (2006) 8217-8226.
40. V. Teixeira, *Thin solid films* **392** (2001) 276-281.
41. S. Fonash, *Journal of applied physics* (1973) **44** 4607.